Investigations on Water Jet Peening of AZ31B Mg Alloy for Bio Medical Implants

Mugilvalavan Mohan
Anna University Chennai
Muruganandhan Radhakrishnan (murugandesign@gmail.com)
Anna University Chennai
Yuvaraj Natarajan
Vel Tech Rangarajan Dr. Sagunthala R&D Institute of Science and Technology

Research Article

Keywords: AZ31-B Mg alloy, TOPSIS, Surface Topography, XRD, Electrochemical Test, SBF Fluid

Posted Date: July 7th, 2021

DOI: https://doi.org/10.21203/rs.3.rs-573898/v1

Abstract

Among different unconventional peening technique, water jet is cold working process has capable to produce surface topography on wide variety of materials. This paper deals with the effect of water jet peening on the corrosion resistance and the surface topography of AZ31B Mg alloy. Variations in water jet peening variables including standoff distance, traverse speed and multiple passes have been employed in this study. A study of the enhancement in hardening and roughening effect was made following the peening process. 29.44% Improvements in microhardness and 31.06% reduction in surface roughness were observed on the peened surfaces. Optimal peened surface was obtained through use of the multi-objective optimization technique, namely, TOPSIS, which utilizes response variables such as micro hardness and surface roughness. In this study, Surface Topography, XRD Analysis and Electrochemical test were conducted. In addition, analysis of the Microstructure of corroded region was made in the unpeened and optimized peened surfaces. Surface topography parameters including S_a, S_q, S_{Sk}, S_{ku} results confirmed the suitability of the peened surface for ooseointegration and cell growth. FWHM value measured from XRD peaks showed the formation of grain refinement on the peened surface, and the results showed promising improvements in the corrosion resistance compared to the unpeened AZ31B Mg alloy.

1. Introduction

Metals are preferred generally for bioimplants like orthopaedics, cardio-vascular stent, dental implants etc [1]. Biomaterials favour the ooseointegration [2] process which mainly depends on surface modification that can enhance the bone to metal implant contact ratio. Currently, Titanium alloy, stainless steel alloy, Chromium based alloys are widely used due to their hardness, high strength, low thermal conductivity and bio-inert nature [3]. However, after a period of years, post-surgical process is needed for the removal of implant which means additional cost, causing damage to tissues. It may take time to heal a surgical wound. So bio degradable material gives greater attention and is preferable to implant. Commercially available magnesium alloys are widely used in automobile and aerospace applications and have attracted the attention of researchers from early 2010’s, due to their bio degradability, biocompatibility, high specific strength and high electrochemical reactivity [4]. Gradual degradation of Magnesium based alloys is seen while therapeutic and total alloys disappear and come-out from the body through the excretory system [5]. Another advantage is the closer proximity of modulus of elasticity to the natural bone which helps attraction towards implants especially orthopaedics.

Among the Magnesium alloys, AZ31B magnesium alloy is recommended, due to its low content of Aluminium which favours the implants as confirmed by previous researchers. Agarwal et al. [6] found the 0–5% of Al content improving corrosion resistance and excess of Aluminium content in physiological environment as harmful with allergic effect to the tissues. Coy et al. [7] have pointed out to the effect of role of Al content. They carried out Laser jet peening on AZ91D magnesium alloys and found enhancement of corrosion resistance. Bannerji et al. [8] have reported poor corrosion performance of LSP ZE41 Mg which has no Al content, indicating the importance of Aluminium presence in Mg alloy [9].

However, AZ31B Mg alloys show rapid and intense corrosion rate in physiological environment [10] leading to adverse effects and harm to tissues during recovery. Enhancement of surface texture is mandatory for the inhibition of corrosion characteristics and for the achievement of better osteoblast with natural bones. Azhari et al. [11] have reported poor surface texture on biomaterials as not suitable for cell growth. Alla [3] and Stanford [12] has reported a roughened surface in the range of R_a 1–10 μm for better ooseointegration and greater than 10 μm macro scale roughness value suitable for dental implants and threads on implant helps to get initial stability. Wennerberg [13] has reported the importance of surface measurements on different scales for getting an understanding of the influence of surface topography on implants.

Different methodologies including alloying, surface coating, surface treatment process for improvement in corrosion resistance and material fatigue strength have been reported. They have produced other potential and biological complications not suitable for implants. Over the years, different surface treatment processes have been suggested for enhancement of fatigue strength and corrosion resistance of the material. These include shot peening, laser jet peening [14], grit blasting and water jet peening [15] [16]. Problems in surface treatment on magnesium alloys have been seen in flame ignition during operations [7]. Metal balls are used in shot peening for impinging on metal surface; This may cause occurrence of crack propagation of the rough peened surface. The use of another surface treatment technique, namely laser peening high pressure shock waves which can help substantial enhancement of residual stress through plastic deformation. But these high-pressure shock waves create heat energy of a large magnitude with possibilities of flame ignition on magnesium-based alloys with the requirement of additional setup or measures to avoid heat generation as reported by Zhang et al. [17]. However, poor surface integrity, formation of contaminants, heat generation hinder the use of these processes in biomaterials [18].

Amongst different unconventional processes, Water jet machining is the promising method for surface modification [19], imparting compressive residual stress [20] in the surface and sub-surface layers for enhancing the fatigue life of material with generation of smaller heat while peening that helps achievement of the desired surface characteristics without affecting the chemical composition of the material. He et al. [1] and Salko [19] have indicated water jet as having potential for improving fatigue strength and removal of residual stress that occur equivalent to the shot peening. Ramulu [21]. Chillman et al. [22] observed a reduction of grain size on Titanium alloy at subsurface level by the employment of water jet pressure of 600MPa. Bagchi et al. [23] have indicated abrasive water jet machine producing higher surface roughness by increasing jet traverse speed. Yuvaraj et al. [24] have reported generation of rough surface pattern on the implant material by the use of abrasive water jet milling. The milled texture could achieve better cell adhesion and load bearing capacity with the use of a body fluid. Bariuso et al. [25] have confirmed the generation of roughened texture on biomaterials like AISI 316 LVM and Ti6Al4V alloys using pure water jet.

The mechanism of waterjet peening process involves the conversion of solid water region into the droplets region. Continuous impingement of high velocity water droplets on the material surface may

result in the development of a higher axial dynamic pressure compared to the LaserJet peening operation due to higher kinetic energy of water jet coming out of the orifice restricting micro cracks on the subsurface of a metal which promotes grain refinement and generate compressive residual stress by localized plastic deformation on the neighbouring surface of the material which improves fatigue strength. Although, many input parameters like standoff distance, water jet pressure, traverse speed, nozzle radius, type of nozzle are involved in the peening process, while control over the input parameters [20] [26] has a predominant role in getting the desired output responses for selected applications.

Reports seen in Literature reveal the capability of water jet to reduce grain size, induce compressive stress and enhance surface texture, but with the requirement of unique parameter setting. Rao [27] has suggested Multi-objective Optimization technique TOPSIS for finding the ideal parameter setting for manufacturing processes. A study of the corrosion inhibiting characteristics and surface Topographical features of peened surface has been made in this work under optimal experimental conditions. Enhancement of surface topography parameters like S_a; S_q; S_{Sk}; S_{ku} was done by Yuvaraj [10] and Xie [28] on metallic implants surface. They have confirmed the potential of water jet in the production of roughened surface in good load-bearing capacity. Yuvaraj [10] also stated compare with smooth surfaces, textured surface topography of implant results better cell growth and interlocking of bone with implant. Consideration of these area parameters is important for surface contact applications such as implants, aerospace, automobile industries. Kalainathan et al. [29] have confirmed improvement of corrosion resistance through use of this peening process on 316L steel. The focus of this paper is on finding the optimal parameter conditions in water jet peening technique for creating a surface pattern with enhanced material properties on AZ31B Magnesium alloy for orthopaedics implant.

2. Materials And Methods

In this study, Mg-AZ31B alloy was selected due to its excellent bio-compatible properties compared to other implant materials. It was used in the plate form with 4 mm thickness and with an elastic modulus of 44.8 GPa, yield and ultimate strength of 200 and 385 MPa respectively, and elongation of 15%. The chemical properties of material are detailed in Table 1. Commercial high pressure water jet machining (Model no: S-3015) Centre was employed for surface modifications on Magnesium alloy. The layout of the experimental setup is shown in Fig. 1. Machining setup is capable of developing water jet pressure up to 350MPa through a high-pressure compressor attached with it. An orifice diameter of 0.30 mm sapphire jewel and tungsten carbide focusing tube with 0.9 mm diameter and 90mm length was used for the entire surface treatments operation.

In this study, high pressure pure water was used for the peening process. Parameter combinations were randomly designed based on the availability of materials. Observations taken related to hardness and surface roughness. 16 different parametric settings trials were designed for peening operations as mentioned in Table 2. Variations in the traverse speed from 1000 to 4000 mm/min, standoff distance from 70 to 150 mm in two successive passes with a water jet pressure of 100 MPa were employed. Peening of Magnesium alloy was conducted at 90^o of the jet impingement angle in the traverse pattern.

Table 1
Composition of Magnesium AZ31B alloy

Element	Mg	Al	Zn	Mn	Si	Cu	Ca	Fe	Ni
%	97	3	0.85	0.2	0.1	0.05	0.04	0.005	0.005

A macroscopic view of peened material surfaces resulting from high pressure pure water jet is shown in the Fig. 2. Micro hardness of water jet peened surfaces was examined using the Wolpert Vickers equipment with 50 gf of load and 10 s dwell period was employed. Details of the influence of water jet peened specimen surface morphology were obtained using contact-type roughness Taly surf tester with a traverse length of 4 mm (5 × 0.8 mm cut-off). Surface topographical profiles and Electrochemical test were taken for selected experimental conditions. 3D surface topography test was done in the peened and unpeened material surfaces using a Taylor Hobson CCI-non contact roughness tester with a magnification of 50x and a working distance of 3.4 mm. These measurements were taken at the top surface area of water jet peened profile with a focused area of 325 μm.

Table 2
Parametric Design of Water jet peening Experiments

Experiment No	Water Jet Pressure (MPa)	Standoff Distance (mm)	Traverse Speed (mm/min)	NOP
Unpeened	Base Material			
PE1	100	70	4000	2
PE2	100	100	4000	2
PE3	100	120	4000	2
PE4	100	150	4000	2
PE5	100	70	3000	2
PE6	100	100	3000	2
PE7	100	120	3000	2
PE8	100	150	3000	2
PE9	100	70	2000	2
PE10	100	100	2000	2
PE11	100	120	2000	2
PE12	100	150	2000	2
PE13	100	70	1000	2
PE14	100	100	1000	2
PE15	100	120	1000	2
PE16	100	150	1000	2

Electrochemical corrosion test was carried out in SBF medium and three-electrode system with AZ31B Magnesium alloy as the working electrode, a platinum wire as the counter electrode and saturated calomel electrode (SCE) as the reference electrode. A working electrode fabricated from AZ31-B Magnesium alloy of 10 mm * 10mm was fixed in the Teflon holder. Earlier, for each electrochemical experiment, this working electrode was cleaned in ethanol mixture in an ultrasonic bath for the removal of impurities, rinsed with water and then dried in air.

Characterization of AZ31B Mg samples was done before and after WJP using an X-ray diffractometer with a wavelength of 1.54 Å and a scanning rate of 0.05^{o} min^{-1}. Simulated Body Fluid (SBF) solution and its pH value 7.4 was used as the electrolyte for electrochemical Corrosion Characterization, which was carried out at room temperature. Details of the ions presented in SBF solution are listed in Table 3. Peened and Unpeened Specimens were immersed in the test solution and Potentio-dynamic polarization

test was carried out in the scanning rate of 0.1667mV/s. The potentio -stat (model PGSTAT 12, Auto lab, Netherlands B.V.) was used for the electrochemical test. This system was interfaced with a personal computer to enable control of analysis of the experiments and data was collected using the dedicated software (GPES version 4.9.005). A Scanning electron Microscope (SEM)- Hitachi (S-3400) was used for the examination on surface micrograph of corroded surface of peened and unpeened specimens in a secondary electron mode with a magnification of 10X and 100X.

Table 3
Concentrations of SBF in Comparison with those in Human Blood Plasma

Ions Concentration	Na^+	K^+	Mg^{2+}	Ca^{2+}	Cl^-	HCO^{3-}	HpO^{4-}	So_4^{2-}
Blood Plasma	142	6.5	1.5	2.5	103	27	1.0	0.4
SBF	142	6.5	1.5	2.5	147.8	4.2	1.0	0.4

3. Results And Discussion

3.1. Variations in surface hardness with different standoff distance at different traverse speed

Micro hardness of base material AZ31-B Mg alloy is 93.7 $HV_{0.05}$. Analysis of measured surface micro-hardness was made at standoff distance(h) = 70mm; 100mm; 120mm; 150mm and traverse speed(v) = 1000mm/min; 2000mm/min; 3000mm/min; 4000mm/min with number of passes = 2 and water jet pressure p = 100 MPa. Table 4. shows the measured micro-hardness and surface roughness values of the peened and Unpeened surfaces of AZ31-B Mg alloy. Figure 3. shows the variations in the measured results on the effect of different standoff distance and traverse speed on the strengthening of material was analyzed. A significant improvement in hardness was observed compared to the base material. Surface hardness showed a tendency to increase with increase in standoff distance to a 132.8 $HV_{0.05}$.

Table 4
Variation of Micro-Hardness and Surface Roughness of Parameter settings

Experiment No	Water Jet Pressure (MPa)	Standoff Distance (mm)	Traverse Speed (mm/min)	NOP	Micro Hardness ($HV_{0.05}$)	Surface Roughness (R_a)
Unpeened	Base Material				93.7	0.962
PE1	100	70	4000	2	110.4	1.1
PE2	100	100	4000	2	116.2	0.977
PE3	100	120	4000	2	112	0.94
PE4	100	150	4000	2	110	0.83
PE5	100	70	3000	2	94.2	1.86
PE6	100	100	3000	2	116.6	1.38
PE7	100	120	3000	2	132.8	1.157
PE8	100	150	3000	2	124.1	0.816
PE9	100	70	2000	2	95.2	3.37
PE10	100	100	2000	2	96.6	2.71
PE11	100	120	2000	2	99.2	1.433
PE12	100	150	2000	2	114.9	0.774
PE13	100	70	1000	2	94.1	8.1
PE14	100	100	1000	2	95.4	4.04
PE15	100	120	1000	2	94.9	1.69
PE16	100	150	1000	2	99.3	0.734

Evaluation of results confirmed the occurrence of improvement of microhardness on the higher standoff distance (h = 70mm to h = 150mm). The maximum micro-hardness recorded was 132.8$HV_{0.05}$ at h = 120mm v = 3000mm/min; NOP = 2. Increase in the standoff distance (h) from 70mm to 150mm, resulted in the impinging of water jet on the target surface in the form of individual clusters of water droplets. This created cyclic water hammer pressure action [28] on the surface which permitted as a compressive load on the subsurface and preceding the movement of dislocation of slip boundaries and planes. This resulted in the maximum gradient of work hardening effect on surface layers.

A gradual increase in the micro-hardness of peened surface was seen from 95.2 $HV_{0.05}$ to 114.9 $HV_{0.05}$ from the traverse speed of nozzle from v = 1000 mm/min to 4000 mm/min at the standoff distance (h) =

70mm and 100mm. This was due to the characteristic of water from the nozzle to the discrete formation of water jet cluster which induced plastic deformation in the subsurface layer. However, at the standoff distance h = 120mm and h = 150mm with traverse speed v = 3000mm/min and v = 4000mm/min, there was a decrease in the micro-hardness of peened region decreases from 132.8 $HV_{0.05}$ to 110 $HV_{0.05}$. This was due to the aerodynamic interaction of water jet, resulting in a substantial reduction on the formation of water droplet cluster, causing variations in axial velocity fluctuation of compression load by water droplets there was also a big reduction in revelation period of interaction of the cluster of water droplets with material surface at higher traverse speed [30]. This confirmed the parametric variant h = 120mm with v = 3000mm/min, that allowed a maximum compressible load on the surface in the form of water droplet clusters, leading to induction of elastic-plastic strain to the subsurface. Above h = 120mm, the intensity of water droplets caused a reduction in the shock pressure wave over the material surface resulting in a smaller deformation effect on the subsurface despite variations in the traverse speed from 1000mm/min to 4000mm/min.

In addition, water jet peening at single pass created small plastic strain along the peening path. When the nozzle moved in ‘S’ shaped path for second passes in the peened region, the step over distance of water jet (D_c) triggered residual stress formation through plastic deformation. But the kinetic energy of the water jet in this second pass with higher in value of step over distance of water jet (D_c=1mm) did not have the ability to influence the plastic deformation on subsurface layer followed by the first pass water jet peening region. A further increase in the number of passes (NOP = 4 and 6), rather than this formation of elastic-plastic strain in subsurface, visible erosion and grooves was observed on the surface level. This was due to the continuous impact of high-pressure water jet on same peening path in the successive passes.

3.2. Variation of surface roughness with different standoff distance at different traverse speed

The effect of variation in the standoff distance on the surface roughness of the peened material at water jet pressure of p = 100MPa with two number of passes is shown in Fig. 4. Initial surface roughness (R_a) of the base material measured was 0.962μm. Following the water jet peening surface treatment process, the maximum surface roughness recorded was 8.1μm at standoff distance (h) = 70mm with traverse speed (v) = 1000mm/min. Decrease in surface roughness value (R_a) with increase in standoff distance (h = 70mm to h = 150mm) at high water jet pressure (p = 100MPa) was seen. This nature of surface was due to the characteristics of water jet under different parametric conditions. Compared to the standoff distance of h = 150mm, the effect of cyclic impact energy of water droplets on the material was quite high in the standoff distance of h = 70mm. This permitted longitudinal and compressive waves to the impact region, initiating compressive longitudinal waves, with the ability to interact with the microstructural discontinuities and resulting in the improvement in the roughness of the material.

With a reduction in the standoff distance(h) from 150mm to 70 mm, there was an increase in the magnitude of individual water droplet energy causing improved roughness (R_a) in the peened region from

0.734μm to 8.1μm. Surface roughness drift was similar at traverse speed (v) with variations from 1000mm/min to 3000mm/min. The maximum average surface roughness value (R_a) was recorded at traverse speeds(v) = 1000mm/min; 2000mm/min; 3000mm/min was 8.1μm; 3.37 μm; 1.86 μm respectively. This similar roughened surface seen by Stanford [12] is suitable for dental implants.

This was due to the exposure period of high-pressure water jet with a material surface. Reduction in traverse speed (v) produced the maximum number of water droplets and caused machining action on the surface. It also created surface abrasion on the material. At a higher standoff distance (h = 150mm), there was reduction in the effect of kinetic energy of water droplet due to the divergence of water jet stream. It forced a smaller effect of cyclic load on the material surface, creating smooth surface roughness value in the range of 0.734 to 0.83, which was 13.2 % lower than the unpeened material surface roughness. This confirmed the absence of occurrence of significant peening action on the surface above a certain standoff distance even at low traverse speed.

The usage of two passes caused a higher hydraulic impact with abrasion in surface asperities with a reduction in the standoff distance. Initial jet passes water jet originated micro cracks without any shearing effect [31] on the material surface and with no formation of greater and deeper craters. There were no changes in the effect of roughness. But, at successive passes start of initiation of some new cracks was seen which easily propagated previous cracks, leading to the removal of an increased material rate at the surface. As a result, a significant improvement in roughness was observed, leading to the combination of surface material erosion and micro cracks leading to material fatigue.

3.3. Multi-response Optimization Technique TOPSIS

Selection of critical factors between different output responses is a tedious process. Inappropriate choice of input responses may lead to surface damage or machining action rather than peening performance. Based on this consideration, selection of optimal input response setting is significant. Amongst different optimization techniques, TOPSIS method is preferable for finding better input responses in manufacturing industries It is closer to the ideal one suggested by Rao [27].

In this study, TOPSIS did relationship assessment between the input responses and the output responses as with the Hardness and Roughness of peened Surface of AZ31 Mg alloy. The basic methodology of TOPSIS involves the choice of input responses that simultaneously find the shortest distance from a Positive Ideal solution that maximizes positive criteria and farthest from a Negative Ideal solution that maximizes negative criteria based on the assumption of weightage to each response. Reference to the steps involved in the TOPSIS has been made by earlier researchers. Table 5, indicates the weightage of Input responses and the ranking of alternatives. The highest closeness coefficient value was obtained under the water jet pressure 100 MPa, SOD = 120mm; TS = 3000mm/min and NOP = 2. Analysis of Surface morphology and topographical features of corroded region of unpeened and PE7 was done for further discussion on the basis of optimal experimental conditions.

Table 5
Weightage of Input Responses and Ranking of Alternatives of TOPSIS

Experiment No	Positive Ideal Solution	Negative Ideal Solution	Closeness Coefficient value	Rank
Unpeened	1.0404	0.0178	0.0169	17
PE1	0.7434	0.3761	0.3359	8
PE2	0.6703	0.5055	0.4300	4
PE3	0.7292	0.4112	0.3606	7
PE4	0.7651	0.3661	0.3236	9
PE5	0.9946	0.0888	0.0819	15
PE6	0.6392	0.5166	0.4470	3
PE7	0.5430	0.8785	0.6180	1
PE8	0.6022	0.6826	0.5313	2
PE9	0.9217	0.2089	0.1848	11
PE10	0.9156	0.1677	0.1548	12
PE11	0.9171	0.1351	0.1284	13
PE12	0.6999	0.4760	0.4048	5
PE13	0.8689	0.5762	0.3987	6
PE14	0.8978	0.2614	0.2255	10
PE15	0.9877	0.0795	0.0745	16
PE16	0.9474	0.1257	0.1172	14

3.4. Effect of optimal parameter setting in 3D surface Topography

The 3D surface topography of the water jet peened surface PE7 was selected using the Multi-objective optimization TOPSIS result, it exposed the peaks and valleys in optimal experiment parametric conditions. Topographical changes were observed from the peened surface as indicated by multiple colours in surface topography as shown in Fig. 5. R_a and R_q are the main parameters to quantify surface roughness for load bearing capacity, but area parameters could provide more information for surface texture. 3D surface parameter values were obtained from the respective peened surface profiles mentioned in Table 6. Surface topology parameters selected in this study were Arithmetic mean height (S_a); Root mean square height value (S_q); Skewness (S_{sk}); Kurtosis (S_{ku}). The focus of the study is on a

surface topography selected for surface contact application like cell adhesion and assessment of the performance of the components.

Graphical results Fig. 6 show, the smooth surface topography obtained in Unpeened over PE7 unpeened surface. This was confirmed by S_a value recorded, namely, 1.459µm to the untreated material surface. A similar surface pattern was reported by Rosa et al. [32] This was due to the effect of the traverse speed(v) 3000mm/min with standoff distance (h) 120mm. It provides threshold energy for a uniform erosion of the materials in the peening region and caused a lower value of roughened surface on the material. Peened region recorded S_q was 2.97µm. This was due to high water jet pressure (p) = 100Mpa with successive passes. It permitted minimum energy for the creation of surface waviness on the peened region [33], leading to the desired roughened surface layer directly associated with the surface energy of the implant and later on affecting the protein absorption and wettability of the surface. Surface wettability enhanced cell adhesion, cell proliferation and prevent premature failure of implant.

Table 6
Variations in Area Parameters of Unpeened and PE7 of AZ31-B Mg alloy

Area Parameters	Unpeened	PE7
Arithmetic mean height	1.718	1.459
Root mean square height	2.35	2.971
Skewness	-0.771	-6.589
Kurtosis	4.244	62.733

S_{sk} parameter describes the shape of the normal height distribution of a roughness profile. S_{sk} -6.589 µm was observed, confirming the surface heights with confined valley structures in the vicinity of the peened region. This was happening due to the effect of traverse speed with high standoff distance in successive passes. At a standoff distance h = 120mm, each water droplet had sufficient kinetic energy for creating surface abrasion in material surface through the removal of material shatters in the minimal level. In addition, traverse speed v = 3000mm/min created a transition region [35] of water jet column that supported the creation of a uniform surface pattern over the peening region. Successive passes induced critical energy of water jet to produce a majority of peaks and valleys closer to the surface of peened region. This combined effect of parameters setting permitted maximum negative skewness values to the unpeened profile. This type of pattern considered favourable for high load bearing capacity provided with a good bonding ratio for any contact type application, was confirmed by the percentage of relative material ratio roughness (Rmr%) shown in Fig. 7. This measured the load bearing and wear resistance of the peened surface. The graph shows improvement in the Rmr value of peened surface over unpeened pattern leads for providing better surface for cell adhesion. This was confirmed by the result obtained by Yuvaraj et al. [10] on-surface milling process on SS304 using AWJ.

Variations in the S_{ku} values for Exp 1 and Exp 8 indicate the uniform presence and absence of peaks and valleys in surface texture. PE7 shows a high Sku value of 62.733µm. This formation confirmed by red colour in Fig. 5, indicates the excessive projection of peaks with deeper valleys are particularly in PE7. This nature of surface created was due to high standoff distance with high traverse speed. It caused a reduction in the intensity of water jet pressure producing inordinate peak and valleys near the peened region.

3.5. Effect of Optimal setting of WJP parameters on XRD Analysis

Figure 8. shows the XRD diffraction patterns of unpeened and peened (PE7) AZ31B Mg alloy at optimized parameter settings. and both the peened and unpeened AZ31B Mg samples as mainly composed of α-Mg while the β-$Mg_{17}Al_{12}$ phase is insignificant, due to the presence of a low content of Aluminium in the alloy. XRD plot show no new diffraction peaks in the peened surface confirming the absence of any new formation of crystals generated after peening. Figure 9. reveals the Intensity of diffraction peak, [002] and [101] of peened surface (PE7) as lower than that of the unpeened surface. Changes in the intensity of the diffraction peaks could be the result of the lower surface finish of the peened surface over the unpeened surface, which became a favourable condition for achieving better ooseointegration and cell growth in body fluid condition. The similar trend obtained by yuvaraj [38] et al. compared the surface integrity of Aluminium alloy with CAAWJM and AWJ cutting process. The position of the diffraction peak at [002] crystalline plane became smooth and was shifted slightly to a higher angle after the WJP process. FWHM values obtained using Jade software data analysis were 0.136^0 and 0.173^0 for unpeened and PE7 surface respectively, obtained using the Jade Software data analysis. The broadened diffraction peak could be the result of grain refinement [37] and an increase in the micro-strain rate on the material surface layer of AZ31B Mg alloy after WJP, which was further confirmed through the estimation of the grain size of peened and unpeened AZ31B Mg surface by Debye-Scherrer formula:

$D = K\lambda/\beta \cos\theta$----------(1)

Where,

D is average crystallite size (nm)

λ stands for X-ray wavelength (0.15046 nm)

β is the FWHM of diffraction peak (radian)

θ is half of diffraction angle (degree)

K is a constant with value set to 0.89 from the XRD experimental data.

Grain sizes for the peened and unpeened surfaces calculated were 43.489nm and 51.263nm respectively, confirming the refinement of the grain size of the Water jet peening treatment without abrasives through

their effect on the surface on a nano scale level through severe plastic deformation [6].

3.6. Effect of Optimal setting of WJP parameters on Corrosion performance

The potentio dynamic polarization curves of Unpeened and PE7 in SBF solution are shown in Fig. 10. Determination of Corrosion potential (E_{corr}), corrosion current density (i_{corr}) and polarization resistance (R_p) was done using the Tafel extrapolation [28][36] method, details are provided in Table 7.

Table 7
Calculated Values of E_{corr}, I_{corr}, and Corrosion Rate of Unpeened and PE7

Experiments	E_{corr} (V)	I_{corr} ($\mu A/cm^2$)	R_P ($\Omega\ cm^2$)	Corrosion rate (µm/Year)
Exp 1	-0.16279	0.013292	$1.5419*10^5$	0.31106
Exp 8	-0.32044	0.004067	$7.4169*10^5$	0.047259

In the case of the Unpeened surface, a sharp rise in cathodic polarization curve with increase in corrosion potential indicating the development of hydrogen evolution and magnesium dissolution was observed. The passive region was confirmed by the anodic branches of the polarization curves, indicating the natural formation form the passive films on the sample surface [7], when the alloy samples were exposed to a corrosive medium.

Tafel behavior was observed for PE7 with surface roughness of 1.157 Ra, and the steady increase in the current on the anodic potential region indicated the WJP AZ31-Mg alloys exhibiting wider passive regions than the as-received ones. PE7 was seen exhibiting its ability to hinder the corrosion effect. This could be the result of the strengthening effect at the grain boundaries due to the WJP process, despite a higher surface roughness value. Grain boundaries are highly susceptible to corrosion as they tend to possess high surface energy creating an anodic region with respect to the grain region. WJP treatment resulted in the refinement of surface and a plentiful grain boundary [25]. The newly developed refined grain boundaries showed a tendency to slow down the corrosion process in comparison with the coarse grain structure [31] due to the presence of Al content in grain boundary, acting as a kinetic barrier [34]. This was confirmed by EDAX result showed a higher presence of Al content in the corroded region of peened over the unpeened surface in Table 8.

PE7 indicates the formation of an immediate passive surface layer which is relatively stable and compact when exposed to SBF solution. The immediate passive layer might cause a reduction in the corrosion rate on AZ31-B Mg alloy due to its increased specific surface area and surface activity over the unpeened surface which slowed down the reaction with chloride ions. This phenomenon was further confirmed through the presence of the wider potentio-dynamic polarization curve for the peened surface as seen in

Fig. 10. A similar trend was observed by Liu et al [19] following the analysis of the corrosion behavior of magnesium alloys using shot peening. Better corrosion inhibiting nature was observed as the effect of surface roughness up to a certain limit, and reduction in the micro galvanic corrosion between the grain boundary and grain region for the WJP surfaces.

Table 8
Presence of Ions in corrode region Unpeened and PE7 in SBF Fluid

Weight %	O	Mg	Al	P	Cl	K	Ca
Unpeened	55.27	39.91	0.42	0.32	2.95	0.19	0.93
PE7	36.49	36.78	2.2	14.34	0.49	0.02	9.69

With increase in the number of passes (NOP = 2) in the case of peening process, there was preponderance of the smooth regions on the corroded surface. There was also a significant reduction in the number of pits compared to the unpeened surface, wherein pit formation was much narrower for the peened surface (PE7). This was confirmed by the microstructure view of corroded region of Unpeened surface and peened surface shown in Fig. 11. These observations, along with the results of the potentio-dynamic polarization measurements, indicate SOD = 120mm; TS = 3000mm/min; NOP = 2, the highest corrosion resistance for the peened surface (PE7) through the WJP process at optimized parameters.

4. Conclusion

Improvisation of corrosion resistance and modification of surface topography features on AZ31-B Mg alloy was done by water jet peening operation through variations in water jet pressure, traverse speed, SOD and the number of passes. Evaluation of Surface characteristics, namely Micro-hardness and surface roughness was done in selected parameter combinations identified using Multi-objective Optimization Technique TOPSIS. The major conclusions are given below:

1. A significant improvement in Micro hardness value on the peened surface up to 29.44% was seen by the work hardening effect with the employment of two successive passes in water jet peening process.
2. The combined effect of stand-off distance of 150 mm, traverse rate of 2000 mm/min with two successive passes at water jet pressure of 100 MPa produced a lower surface roughness of 0.774 R_a.
3. Despite the presence of lower surface roughness, Multi-objective Optimization Technique TOPSIS was used for obtaining the optimal parameter combinations for the achievement of a surface pattern for implant applications and improvement in corrosion performance in SBF Fluid. The parameter combination under Optimal condition was water jet pressure 100 MPa, SOD 120 mm, Traverse speed 3000 mm/min with two successive passes.
4. The 3-D surface topographical parameters, namely, S_a; S_q; S_{sk}; S_{ku}, proved the formation of better surface contact applications with restraints under different conditions of WJP surfaces.

5. 2D surface roughness of % of Rmr confirmed the possibility of load bearing capabilities, cell adhesion on selected peened surface of AZ31B Mg alloy.
6. XRD Diffraction pattern confirmed the possibility of Grain refinement on selected Peened surface based on the broadening of peak and a slight peak shift towards right side.
7. Tafel Polarization curves indicated the improvement in corrosion performance of water jet peening process with constraint in the parameter conditions.
8. Microstructure analysis of Corroded region of the selected peened surface revealed the presence of Al content in grain boundaries of α matrix of AZ31-B Mg alloy hinders the corrosion effect in SBF Fluid.

The above studies confirm the usefulness of the selected condition of water jet peened surface for implant, particularly in orthopaedics demanding the enhanced ooseointegration and cell growth through a roughened texture. Invitro studies of water jet peened surface will be explored in the near future.

Declarations

Acknowledgments

M. Mugilvalavan acknowledge the Centre for Research, Anna University, Chennai for providing financial Assistance under the scheme of Anna Centenary Research Fellowship (Ref.no.CFR/ACRF-2019/AR1) for this research work.

Funding

Not Applicable

Competing interests

The authors declare no competing interests.

Availability of data and material

Not Applicable

Code availability

Not Applicable

Ethical approval

Our research does not involve humans and animals, so there is no need to provide ethical approval.

Consent to participate and publish

All authors agreed to participate and publish.

Authors' contributions

Mugilvalavan Mohan: methodology, experiments, data analysis, investigation, writing-original draft. Muruganandhan Radhakrishnan: conceptualization, investigation, writing-review and editing. Yuvaraj Natarajan: Investigation, data analysis, writing-review and editing.

References

1. He, Z., Yu, H., Zhao, S., Xing, J., Li, D., Li, C., ... & Wang, S. (2020). An experimental and numerical analysis of water jet peening of Al6061-T6. The International Journal of Advanced Manufacturing Technology, 107(9), 3833-3845.
2. Soyama, H. (2019). Comparison between the improvements made to the fatigue strength of stainless steel by cavitation peening, water jet peening, shot peening and laser peening. Journal of Materials Processing Technology, 269, 65-78.
3. Alla, R. K., Ginjupalli, K., Upadhya, N., Shammas, M., Ravi, R. K., & Sekhar, R. (2011). Surface roughness of implants: a review. Trends in Biomaterials and Artificial Organs, 25(3), 112-118.
4. Hong, K., Park, H., Kim, Y., Knapek, M., Minárik, P., Máthis, K., ... & Choe, H. (2019). Mechanical and biocorrosive properties of magnesium-aluminum alloy scaffold for biomedical applications. Journal of the mechanical behavior of biomedical materials, 98, 213-224.
5. Staiger, M. P., Pietak, A. M., Huadmai, J., & Dias, G. (2006). Magnesium and its alloys as orthopedic biomaterials: a review. Biomaterials, 27(9), 1728-1734.
6. Agarwal, S., Curtin, J., Duffy, B., & Jaiswal, S. (2016). Biodegradable magnesium alloys for orthopaedic applications: A review on corrosion, biocompatibility and surface modifications. Materials Science and Engineering: C, 68, 948-963.
7. Coy, A. E., Viejo, F., Garcia-Garcia, F. J., Liu, Z., Skeldon, P., & Thompson, G. E. (2010). Effect of excimer laser surface melting on the microstructure and corrosion performance of the die cast AZ91D magnesium alloy. Corrosion Science, 52(2), 387-397.
8. Banerjee, P. C., Raman, R. S., Durandet, Y., & McAdam, G. (2011). Electrochemical investigation of the influence of laser surface melting on the microstructure and corrosion behaviour of ZE41 magnesium alloy–An EIS based study. Corrosion Science, 53(4), 1505-1514.
9. Lieblich, M., Barriuso, S., Ibáñez, J., Ruiz-de-Lara, L., Díaz, M., Ocaña, J. L., ... & González-Carrasco, J. L. (2016). On the fatigue behavior of medical Ti6Al4V roughened by grit blasting and abrasiveless waterjet peening. Journal of the mechanical behavior of biomedical materials, 63, 390-398.
10. Yuvaraj, N., Pavithra, E., & Shamli, C. S. (2020). Investigation of surface morphology and topography features on abrasive water jet milled surface pattern of SS 304. Journal of Testing and Evaluation, 48(4).
11. Azhari, A., Schindler, C., Kerscher, E., & Grad, P. (2012). Improving surface hardness of austenitic stainless steel using waterjet peening process. The International Journal of Advanced Manufacturing Technology, 63(9-12), 1035-1046.

12. Stanford, C. M. (2008). Surface modifications of dental implants. Australian dental journal, 53, S26-S33.
13. Wennerberg, A. (1998). The importance of surface roughness for implant incorporation. International Journal of Machine Tools and Manufacture, 38(5-6), 657-662.
14. Ge, M. Z., & Xiang, J. Y. (2016). Effect of laser shock peening on microstructure and fatigue crack growth rate of AZ31B magnesium alloy. Journal of Alloys and Compounds, 680, 544-552.
15. Lee, H. S., Kim, D. S., Jung, J. S., Pyoun, Y. S., & Shin, K. (2009). Influence of peening on the corrosion properties of AISI 304 stainless steel. Corrosion science, 51(12), 2826-2830.
16. Saptaji, K., Gebremariam, M. A., & Azhari, M. A. B. M. (2018). Machining of biocompatible materials: a review. The International Journal of Advanced Manufacturing Technology, 97(5), 2255-2292.
17. Zhang, R., Zhou, X., Gao, H., Mankoci, S., Liu, Y., Sang, X., ... & Ye, C. (2018). The effects of laser shock peening on the mechanical properties and biomedical behavior of AZ31B magnesium alloy. Surface and Coatings Technology, 339, 48-56.
18. Salko D. Peening by water. Proceedings of the 2nd International Conference on Shot Peening; 1994; Chicago, IL, USA. p.37–38.
19. Liu, C., Zheng, H., Gu, X., Jiang, B., & Liang, J. (2019). Effect of severe shot peening on corrosion behavior of AZ31 and AZ91 magnesium alloys. Journal of Alloys and Compounds, 770, 500-506.
20. Mahmoudi, A. H., Jamali, A. M., Salahi, F., & Khajeian, A. (2020). Effects of water jet peening on residual stresses, roughness, and fatigue. Surface Engineering, 1-10.
21. Ramulu, M., Kunaporn, S., Arola, D., Hashish, M., & Hopkins, J. (2000). Waterjet machining and peening of metals. J. Pressure Vessel Technol., 122(1), 90-95.
22. Chillman, A., Ramulu, M., & Hashish, M. (2007). Waterjet peening and surface preparation at 600 MPa: A preliminary experimental study.
23. Bagchi, A., Srivastava, M., Tripathi, R., & Chattopadhyaya, S. (2020). Effect of different parameters on surface roughness and material removal rate in abrasive water jet cutting of Nimonic C263. Materials Today: Proceedings, 27, 2239-2242.
24. Natarajan, Y., Murugesan, P. K., Mohan, M., & Khan, S. A. L. A. (2020). Abrasive water jet machining process: a state of art of review. Journal of Manufacturing Processes, 49, 271-322.
25. Barriuso, S., Lieblich, M., Multigner, M., Etxeberria, I., Alberdi, A., & González-Carrasco, J. L. (2011). Roughening of metallic biomaterials by abrasiveless waterjet peening: Characterization and viability. Wear, 270(9-10), 634-639.
26. Muruganandhan, R., Mugilvalavan, M., Thirumavalavan, K., & Yuvaraj, N. (2018). Investigation of water jet peening process parameters on AL6061-T6. Surface Engineering, 34(4), 330-340.
27. Rao, R. V. (2007). Decision making in the manufacturing environment: using graph theory and fuzzy multiple attribute decision making methods. Springer Science & Business Media.
28. Xie, J., & Rittel, D. (2018). The effects of waterjet peening on a random-topography metallic implant surface. European Journal of Mechanics-A/Solids, 71, 235-244.

29. Kalainathan, S., Sathyajith, S., & Swaroop, S. (2012). Effect of laser shot peening without coating on the surface properties and corrosion behavior of 316L steel. Optics and Lasers in Engineering, 50(12), 1740-1745.
30. Azhari, A., Schindler, C., Godard, C., Gibmeier, J., & Kerscher, E. (2016). Effect of multiple passes treatment in waterjet peening on fatigue performance. Applied Surface Science, 388, 468-474.
31. Aung, N. N., & Zhou, W. (2010). Effect of grain size and twins on corrosion behaviour of AZ31B magnesium alloy. Corrosion Science, 52(2), 589-594.
32. Rosa, M. B., Albrektsson, T., Francischone, C. E., Schwartz Filho, H. O., & Wennerberg, A. (2012). The influence of surface treatment on the implant roughness pattern. Journal of Applied Oral Science, 20(5), 550-555.
33. Wu, T. C., Ho, Y. H., Joshi, S. S., Rajamure, R. S., & Dahotre, N. B. (2017). Microstructure and corrosion behavior of laser surface-treated AZ31B Mg bio-implant material. Lasers in medical science, 32(4), 797-803.
34. Bagherifard, S., Hickey, D. J., Fintová, S., Pastorek, F., Fernandez-Pariente, I., Bandini, M., ... & Guagliano, M. (2018). Effects of nanofeatures induced by severe shot peening (SSP) on mechanical, corrosion and cytocompatibility properties of magnesium alloy AZ31. Acta biomaterialia, 66, 93-108.
35. Srivastava, M., Tripathi, R., Hloch, S., Chattopadhyaya, S., & Dixit, A. R. (2016). Potential of using water jet peening as a surface treatment process for welded joints. Procedia Engineering, 149, 472-480.
36. Ezhilselvi, V., Nithin, J., Balaraju, J. N., & Subramanian, S. (2016). The influence of current density on the morphology and corrosion properties of MAO coatings on AZ31B magnesium alloy. Surface and Coatings Technology, 288, 221-229.
37. Yun, Z. O. U., Zhenkuan, S. A. N. G., Qilong, W. A. N. G., Tingchao, L. I., Dalei, L. I., & Yang, L. I. (2020). Improving the mechanical properties of 304 stainless steel using waterjet peening. Materials Science, 26(2), 161-167.
38. Yuvaraj, N., & Kumar, M. P. (2016). Cutting of aluminium alloy with abrasive water jet and cryogenic assisted abrasive water jet: A comparative study of the surface integrity approach. Wear, 362, 18-32.

Figures

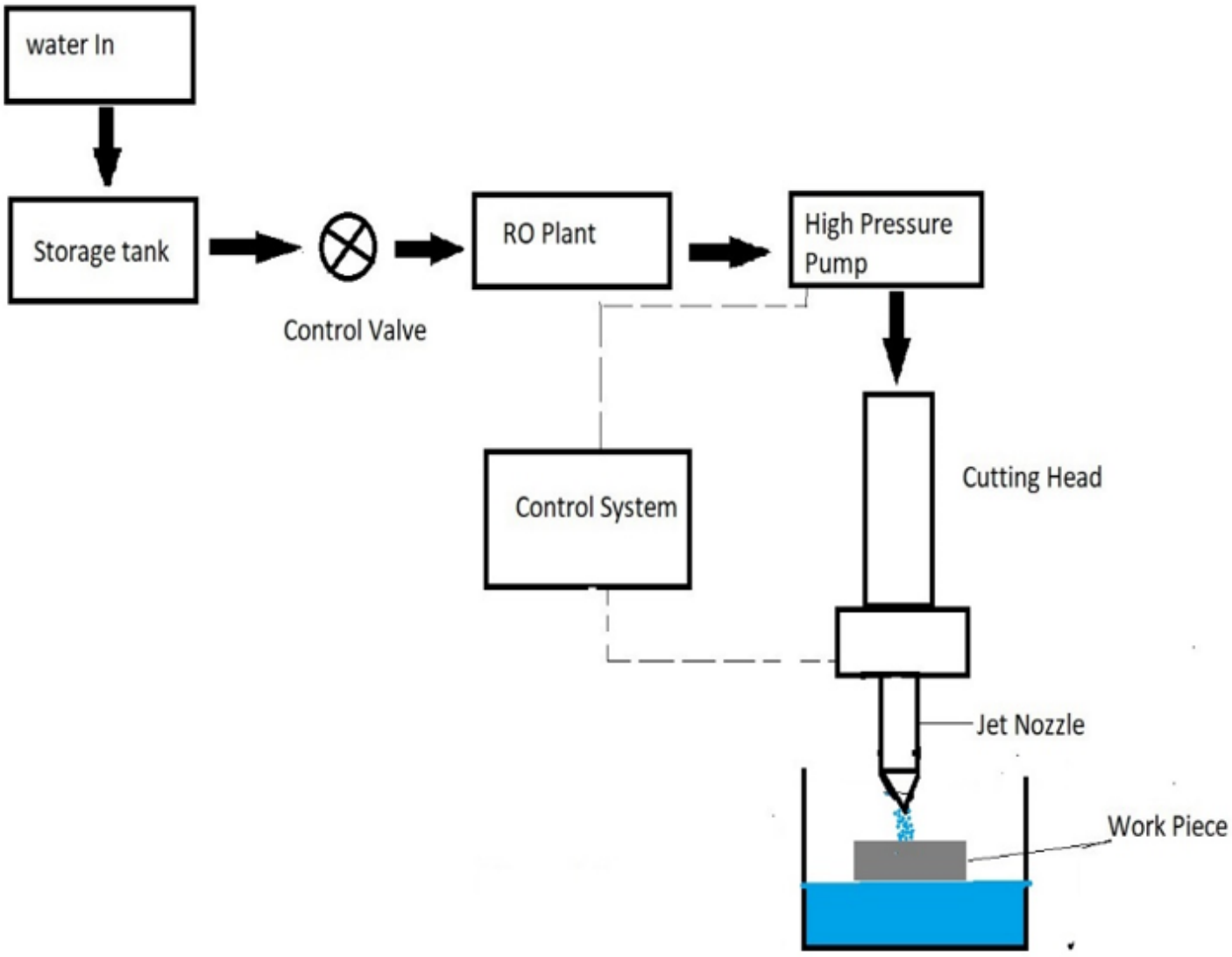

Figure 1

Schematic Diagram of water jet peening setup

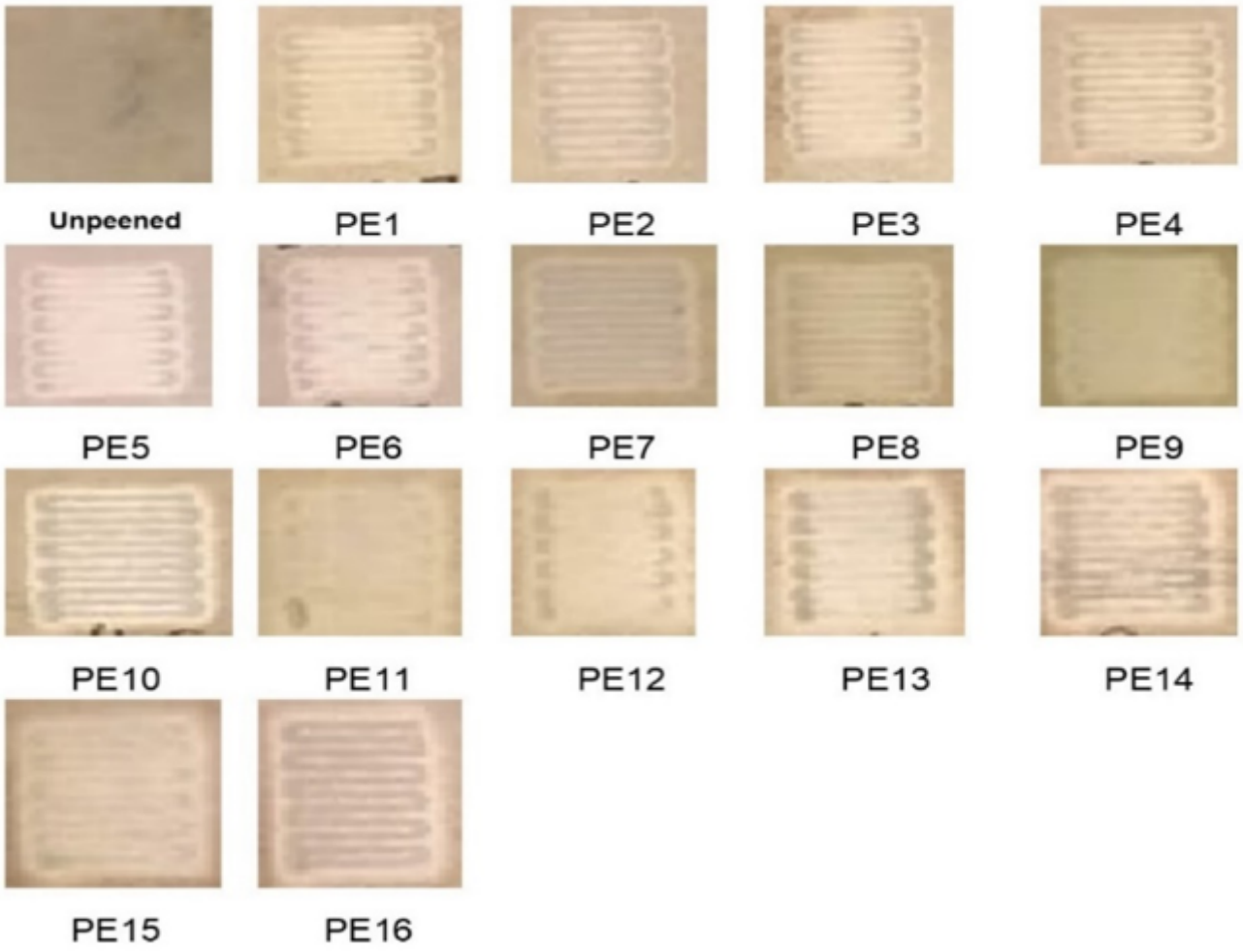

Figure 2

Water-jet Peened pattern on the surface of Mg AZ31 alloy

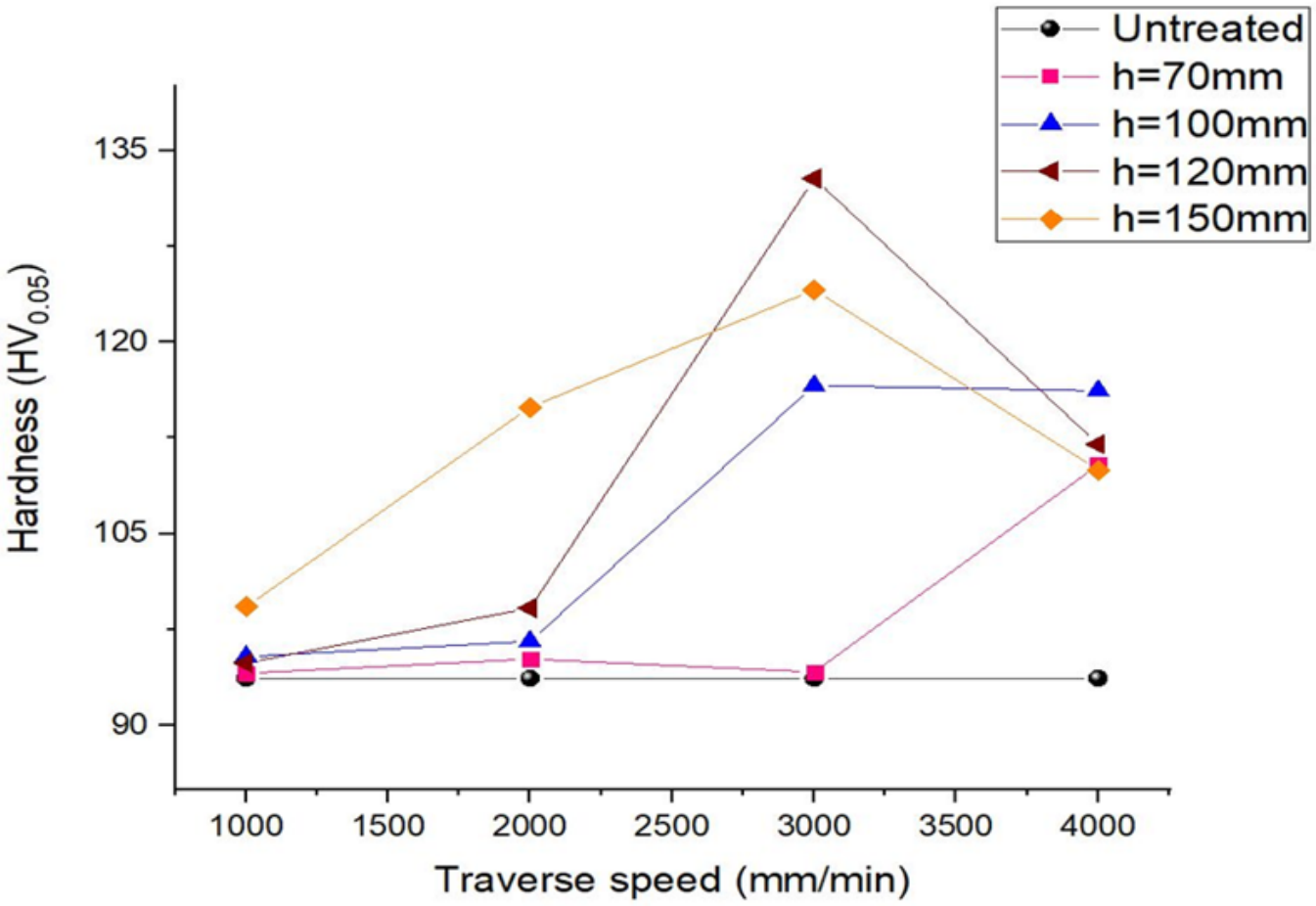

Figure 3

Effect of hardness at different standoff distanceh=70mm;100mm;120mmm;150mm

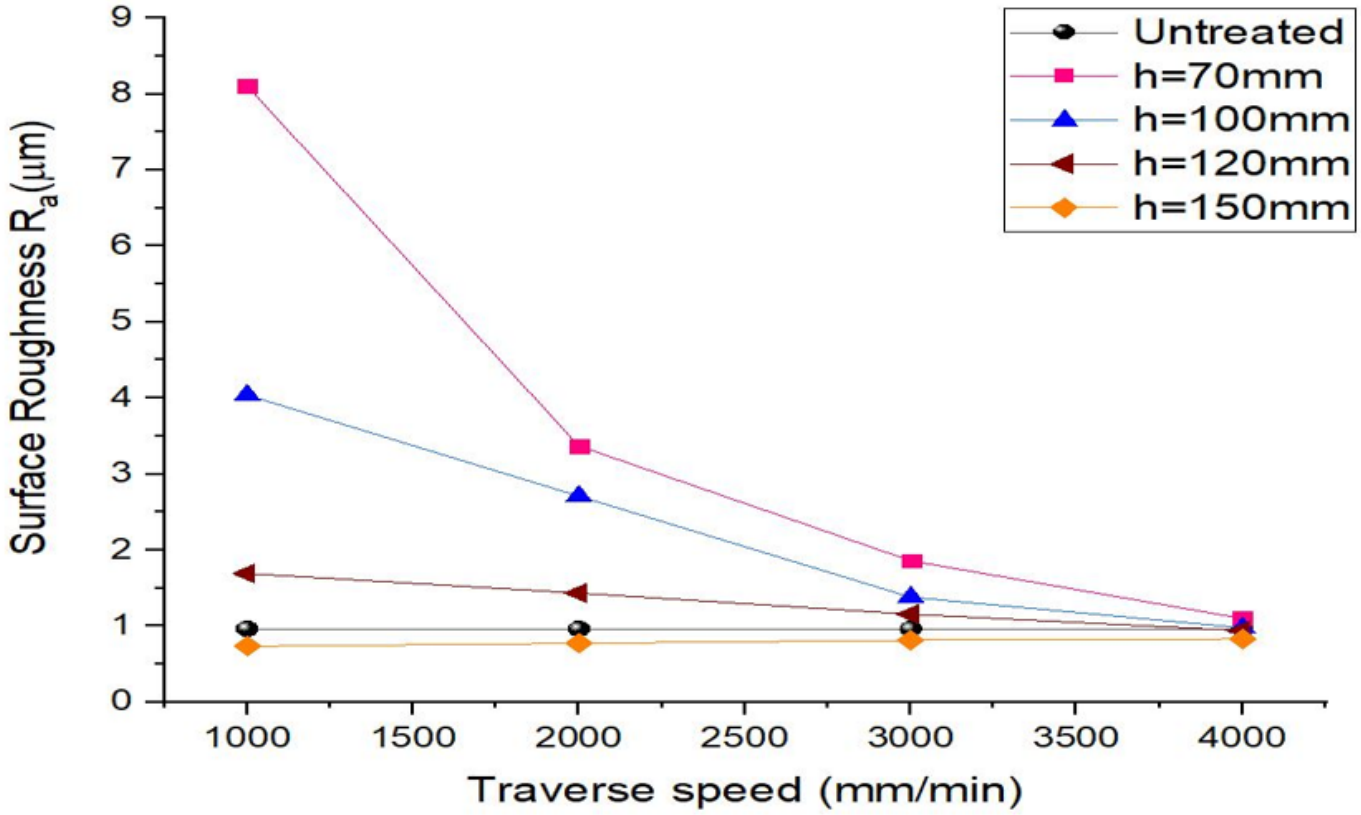

Figure 4

Effect of Ra at different SOD h=70mm; h=100mm; h=120mm; h=150mm.

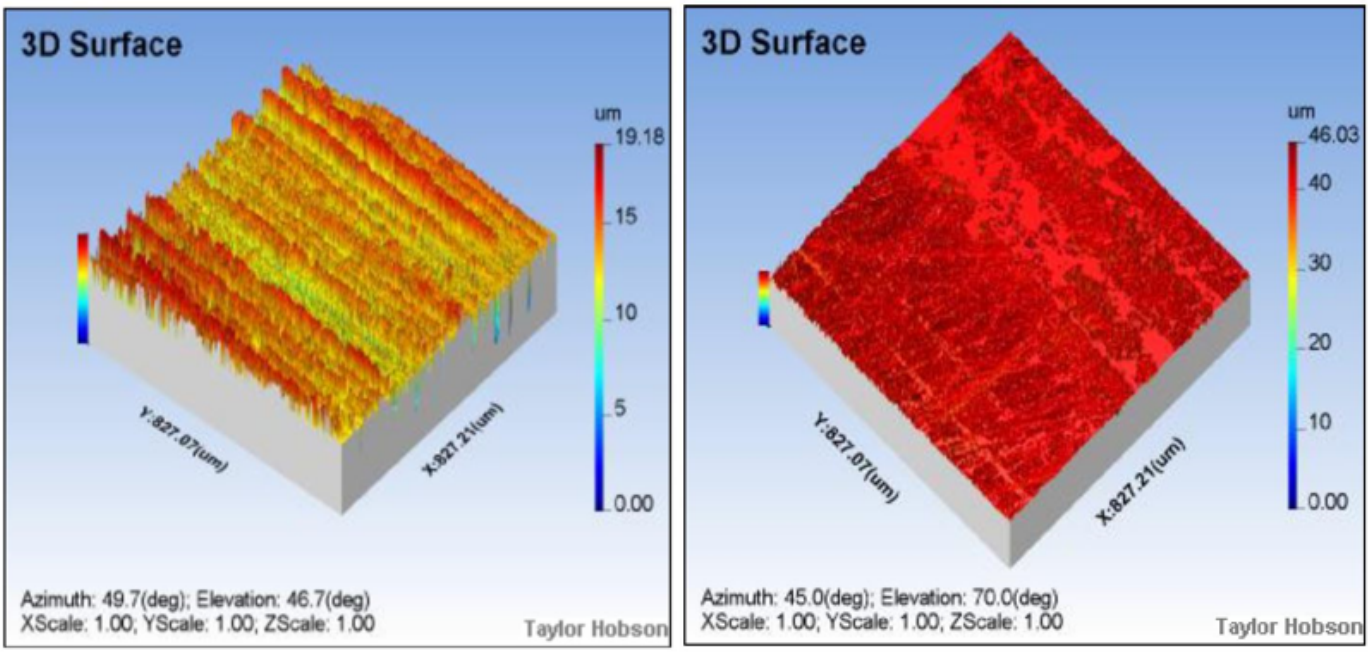

(a) (b)

Figure 5

3d surface topography of a) Unpeened and b) PE7 of AZ31-B Mg Alloy

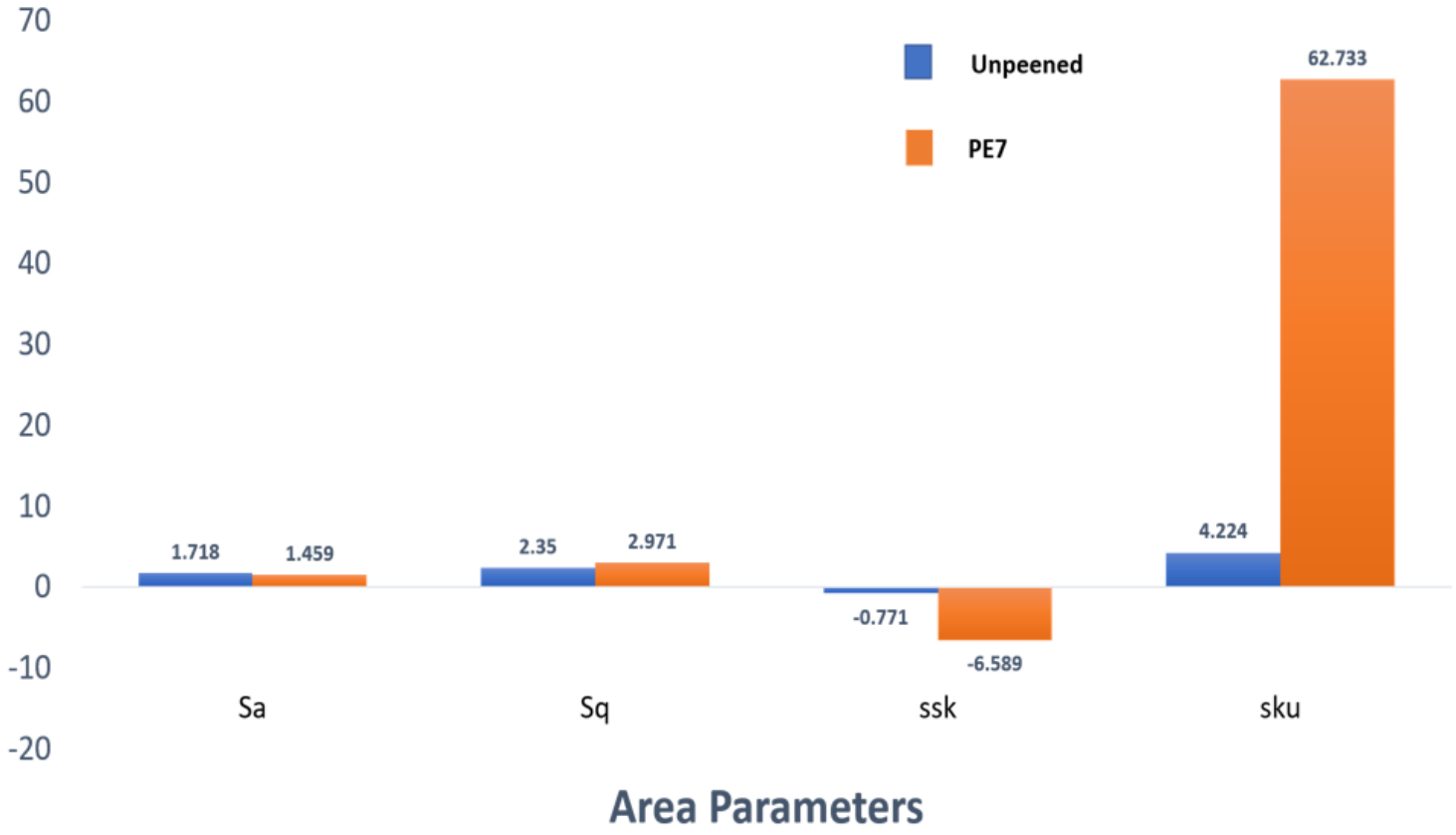

Figure 6

Comparison of Area Parameters of Unpeened and PE7 of AZ31B Mg alloy

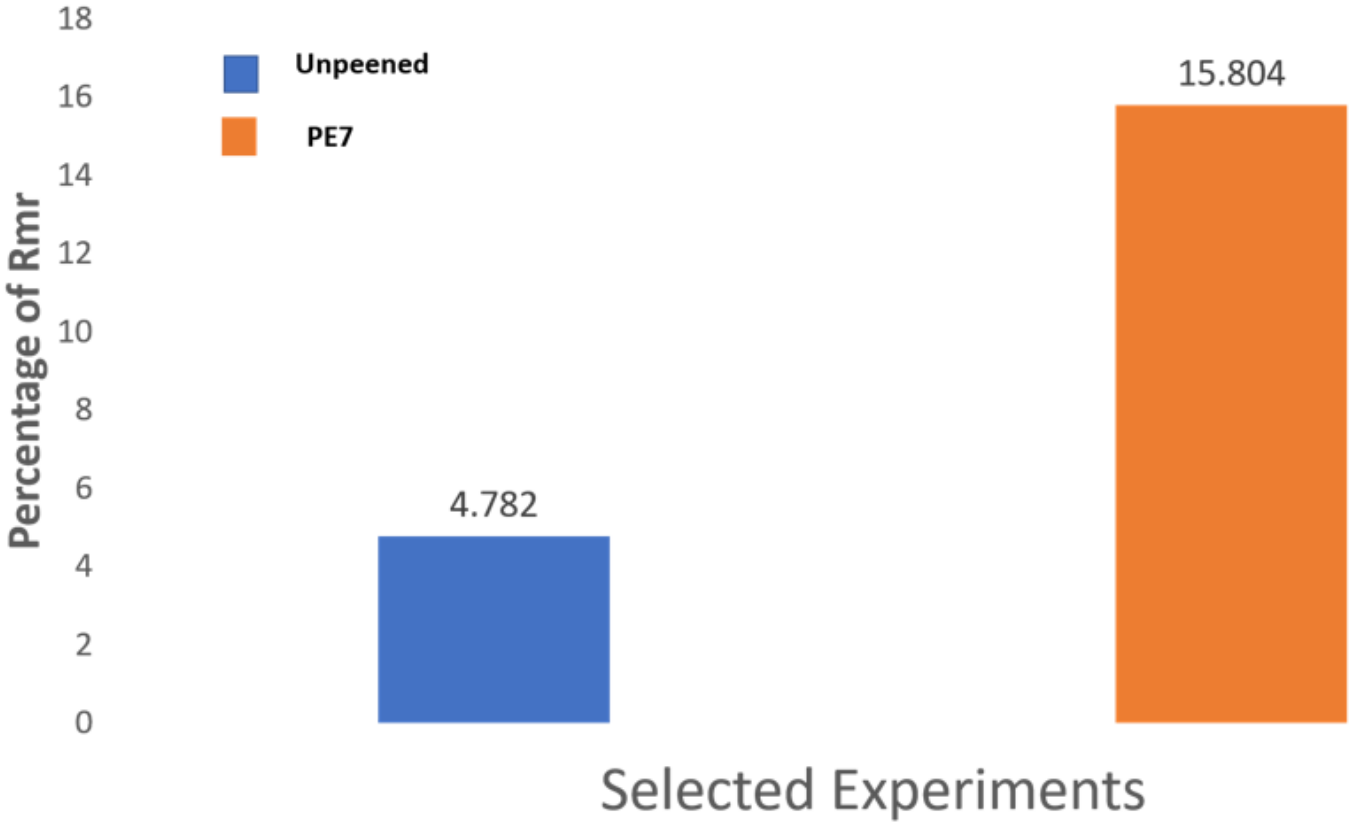

Figure 7

Percentage of Rmr of Unpeened and PE7 of Az31-B Mg alloy

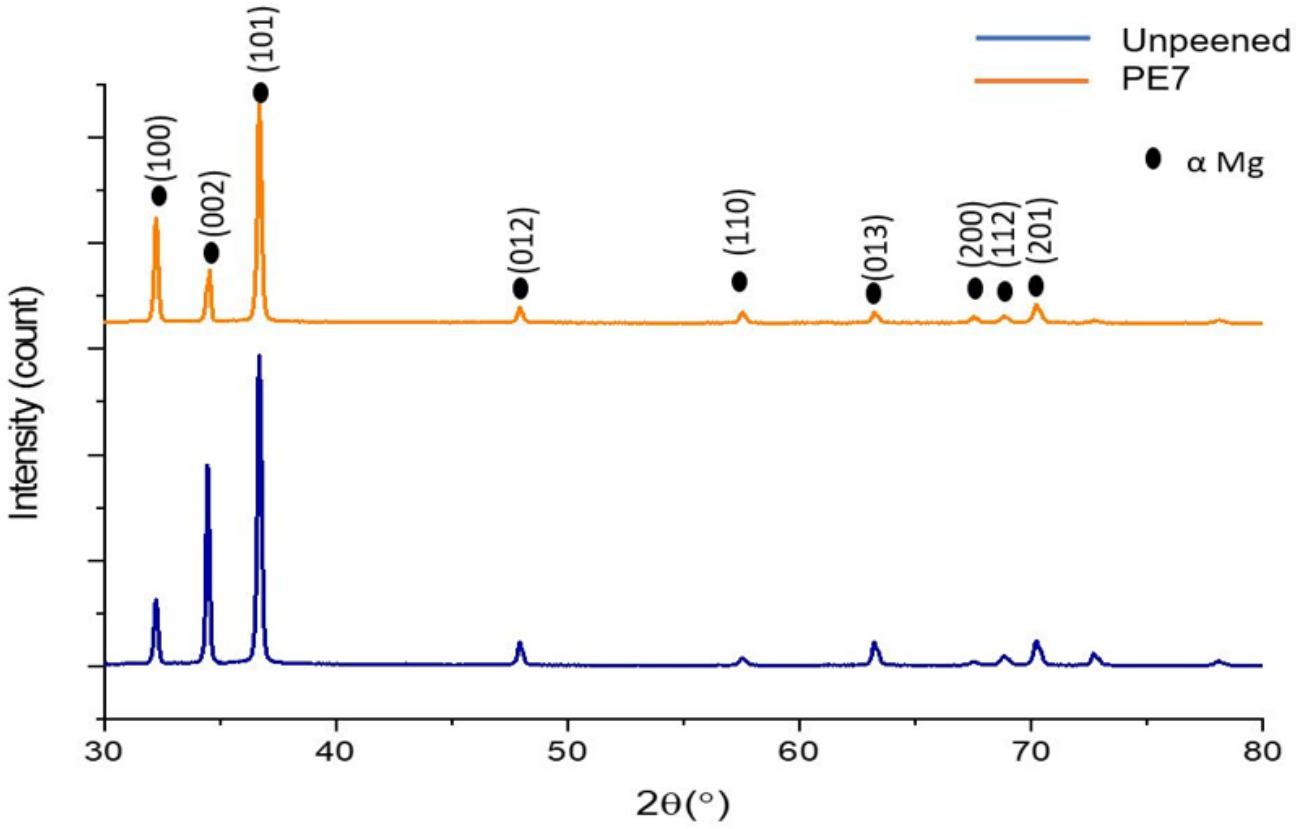

Figure 8

XRD Diffraction Pattern of Unpeened and PE7 of AZ31-B Mg alloy

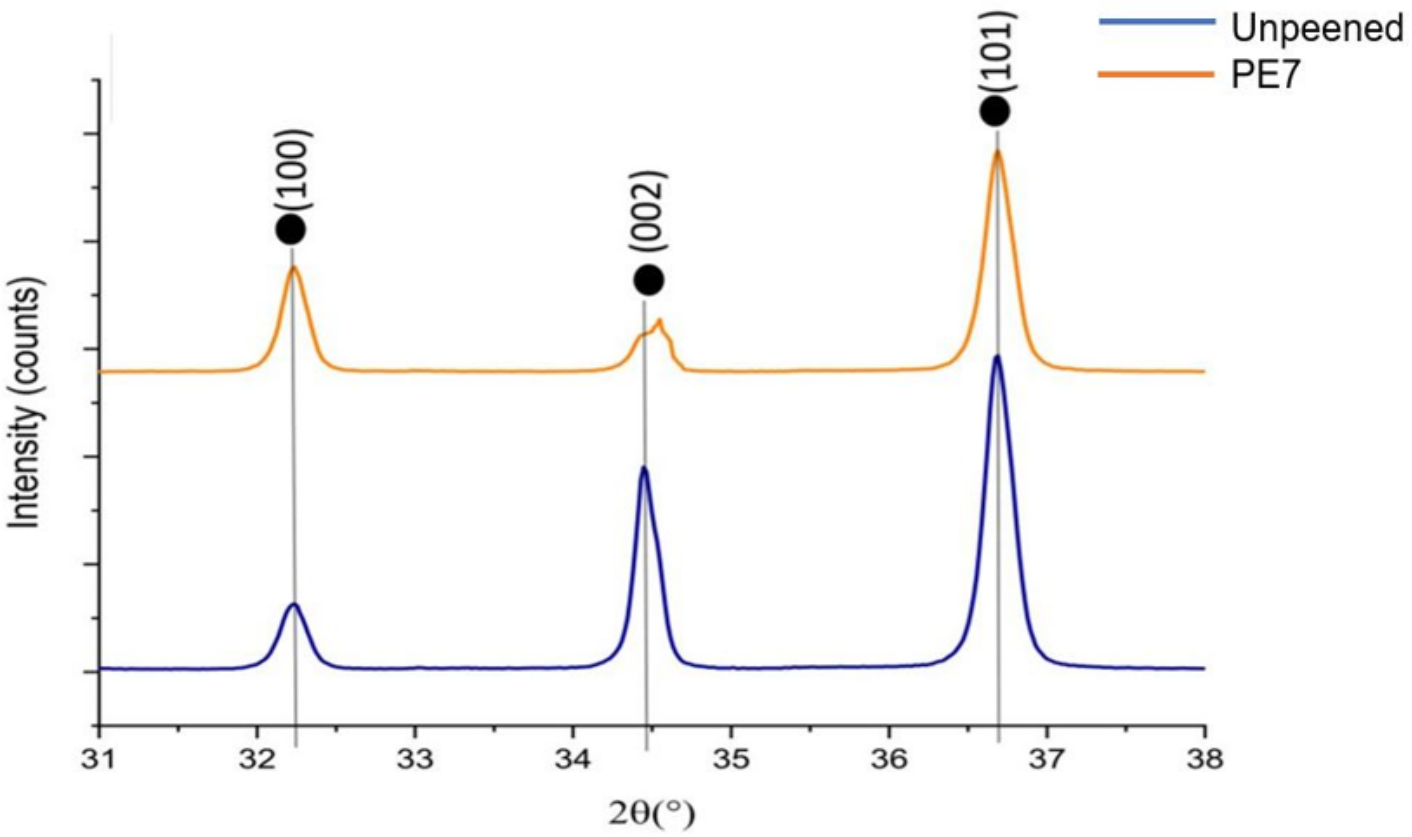

Figure 9

Enlarged XRD Diffraction Pattern of Unpeened and PE7 of AZ31-B Mg alloy

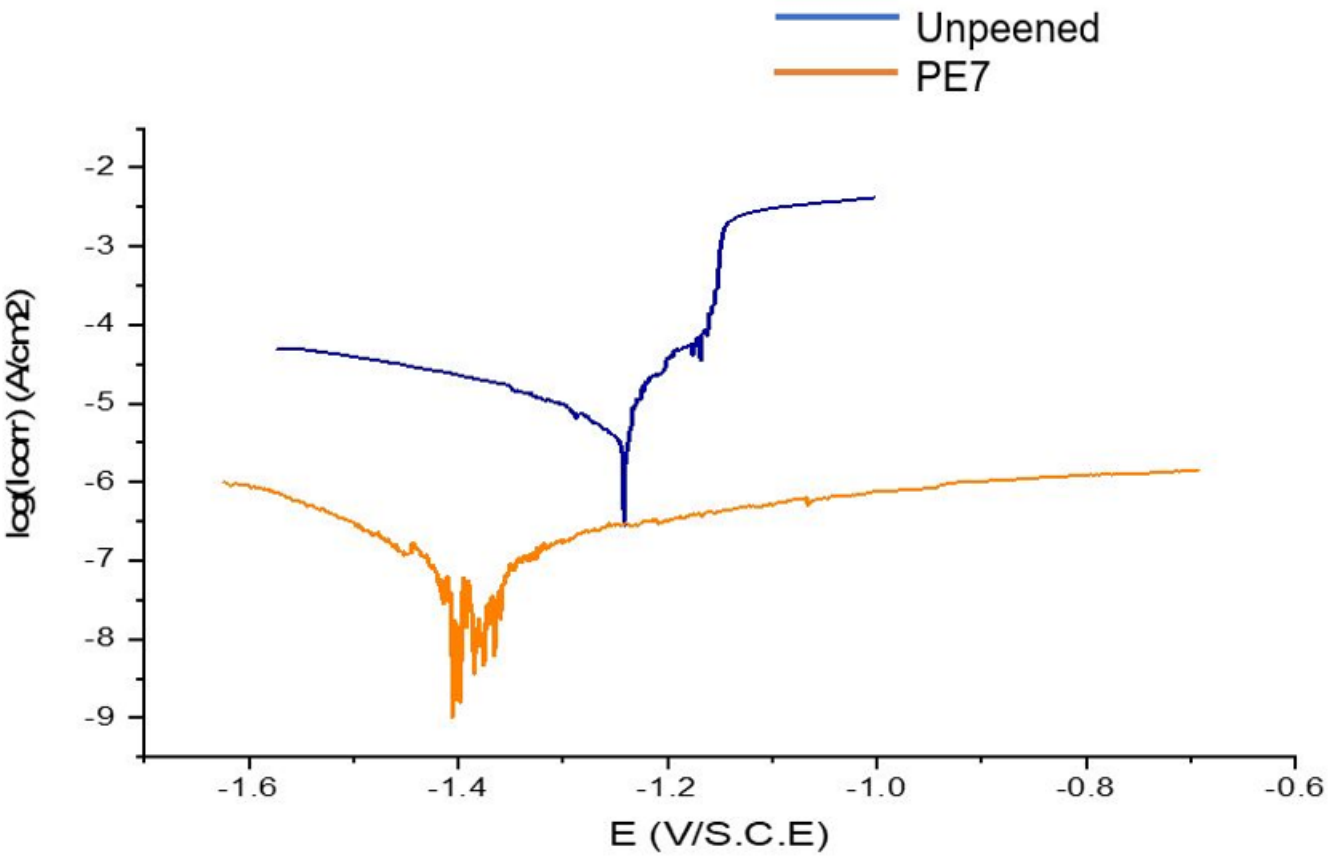

Figure 10

Polarization curve of Unpeened and PE7 in SBF Fluid